Journal of Radioanalytical and Nuclear Chemistry (2022) 331:5287–5295
https://doi.org/10.1007/s10967-022-08477-w

Performance of borated scintillator screens for high-resolution neutron imaging

Burkhard Schillinger[1] · William Chuirazzi[2] · Aaron Craft[2] · Steven Cool[3] · Alessandro Tengattini[4,5]

Received: 29 April 2022 / Accepted: 2 August 2022 / Published online: 6 September 2022

Abstract
The most commonly used screens for neutron imaging consist of ^{6}LiF + ZnS. This type of screen yields the highest light output per detected neutron. For high resolution, gadolinium oxysulfide (GOS, Gadox) screens are employed, which have a much higher detection efficiency, but a light output so much lower than LiF + ZnS that measurements are often limited by photon statistics. Historically, screens using boron as a neutron-sensitive material have not been very successful. However, a new preparation method was introduced recently that produces light output higher than Gadox with detection efficiency greater than LiF + ZnS. Measurements of these new borated screens were performed at the NeXT facility at ILL, Grenoble, in comparison to a high resolution Gadox screen.

Keywords Neutron imaging · Scintillation screen · Neutron converter · Spatial resolution · Light output · Boron · Boron-10 · 10B

Introduction

As neutral particles, thermal and cold neutrons can only be detected by a nuclear capture reaction. Such a capture reaction usually releases a lot of energy, appearing as kinetic energy of the reaction products, which gives them considerable range in a mixture with scintillating material. That range produces an extended light spot per detected neutron that limits the achievable resolution. An ideal screen would have high detection efficiency, high light output and high spatial resolution.

The most commonly employed scintillation screens for neutron radiography use zinc sulfide (ZnS, doped with Ag, Au or Cu for color) mixed with ^{6}LiF with the reaction [1, 2] ^{6}Li(n,α)^{3}H + 4.78 MeV (938 barn). The energy of this reaction appears as kinetic energy in the resulting alpha and tritium particles, which cause scintillation in the ZnS crystal powder. The typical range after multiple collisions is around 70 µm, which causes an extended light spot of at least that approximate size, limiting the resolution of a radiography screen. If all energy is deposited, the light output is on the order of 177,000 photons going into 4π space [1]. Slightly higher resolution can be achieved by using thinned screens, at the cost of reduced efficiency and increased graininess.

At high-flux neutron sources, Gadox screens made of gadolinium oxysulfide (Gd_2O_2S, doped with Tb or Pr) are also employed, using the reaction ^{157}Gd(n,e-)Gd + 71 keV (e-) + γ-cascade up to 8 MeV. Gadox is a scintillator itself, which is mostly used for X-ray and gamma detection, and thus also has a high sensitivity for the gamma content present in almost all neutron beams [2, 3]. However, due to the low energy of the main conversion electrons from neutron capture in ^{157}Gd (29 keV + 71 keV), the range of the reaction products in Gadox is very low, on the order of a few micrometers. Also the light yield from the smaller deposition energy is much less than that of ^{6}LiF in zinc sulfide, only 3.29 photons per neutron capture on average [4]. Due to the much higher cross section of Gd and thus much higher detection efficiency, screens can be thinned to 10–20 µm for

✉ Burkhard Schillinger
Burkhard.Schillinger@frm2.tum.de

1 Heinz Maier-Leibnitz Zentrum (FRM II), Technische Universität München, Lichtenbergstr.1, 85748 Garching, Germany

2 Idaho National Laboratory, PO Box 1625, Idaho Falls, ID 83415, USA

3 DMI/Reading Imaging, Reading, MA 01867, USA

4 Institut Laue-Langevin, Grenoble, France

5 CNRS, Grenoble INP, 3SR, University Grenoble Alpes, 38000 Grenoble, France

nearly full absorption, delivering a resolution about equal to the range of the thickness. At medium to low neutron flux, the low light yield is a challenge for camera detectors which cannot capture photons from every neutron event, resulting in noisy images due to poor photon statistics. A possible path towards high resolution with higher light output would be to use a capture reaction that produces heavier reaction products with shorter range within ZnS.

Boron-based screens

Compared to ^{6}Li, the capture reaction ^{10}B(n,α)^{7}Li (3855 barns) produces less kinetic energy (2.31 MeV) distributed on the alpha particle and the much heavier ^{7}Li, which have a much lower combined range. A well composed scintillation screen might use boron combined with ZnS, combining smaller spot size than from LiF, and higher light output than from Gadox. However, earlier reports about trial screens containing boron showed much lower light output than expected, to an extent that made those screens practically unusable. Simulations performed in [4] showed the range of the reaction products to be on the order of only 2–3 µm in any boron-containing substance, as shown in Table 1.

Since the 1950s, boron-based scintillators have been proposed [5] and their improved detection efficiency has been proven [6]. Boron-based scintillators have been deployed in the form of glass [7–9] and plastic scintillators [10–13]. However, in previous attempts at creating boron-based scintillator screens [14–16], mixtures of boron-containing powders and ZnS powder had grain sizes on the order of many micrometers, so the reaction products hardly had a chance to escape their grain if they were not created close to the surface. The key therefore lies in very fine milling of the boron-containing powders, to minimize self-shielding of the daughter products produced in the powders.

Several finely milled substances such as ^{10}B-enriched boron powder, ^{10}B-enriched boric acid, ^{10}B-enriched sodium pentaborate, Boron Oxide, Boron Nitride, Wurtzite-Boron Nitride and Anhydrous Sodium Tetraborate were tried out in a first set of measurements at the ANTARES facility [17] of the FRM II reactor of Technische Universität München, Germany, in 2019/2020, which were published in [4].

These first measurements used wedge-shaped screens of 0–200 µm thickness to test screen's light output dependence on thickness. For these first measurements, detector resolution was low to achieve a large field of view for simultaneous measurement of many screens. The best-performing substances were milled into fine powders and used to fabricate screens of 20 µm thickness. Due to the continued shutdown of the FRM II reactor, they were measured at the NeXT facility of the reactor at Institut Laue-Langevin (ILL) in Grenoble [18] in 2021.

Measurements

The NeXT instrument is situated at the end of a cold neutron guide, followed by a 5 m long flight tube. Variable apertures at the beginning of the flight tube can set the collimation. The beam has a very pure cold neutron spectrum due to the curved neutron guide, which eliminates fast neutrons and gamma radiation from the reactor. A 90° Heliflex lens is used to image the scintillation screens, keeping the cooled Hamamatsu ORCA-Flash4.0 V2 sCMOS camera out of the beam (Fig. 1). Initial tests were made with an effective pixel size of ~ 7.15 µm. Figure 2 shows the measurement of a gadolinium Siemens star as a test pattern with about 7.15 µm effective pixel size using screens made of boron oxide ($^{10}B_2O_3$) and sodium pentaborate ($Na^{10}B_5O_8$) mixed with ZnS:Cu. The rings correspond to 500, 400, 300, 200, 100 and 50 µm for a line pair of spokes on the ring. A more accurate set of measurements used a detector setting of 3.6 µm effective pixel size to determine the resolution, as shown below in Fig. 3. Shown is the inner ring corresponding to 50 µm for a line pair of spokes (25 µm for one line), and the outer edge of the dot corresponds to 8 µm per line pair, 4 µm for a line width.

Table 1 Ranges of reaction products inside the converter material, amended from [4]

Converter	Density (g/cm^3)	Daughter product range			
		^{7}Li (1.01 MeV)	α (1.78 MeV)	^{7}Li (0.84 MeV)	α (1.47 MeV)
$^{10}B_2O_3$	2.46	2.45 µm	4.84 µm	2.19 µm	3.97 µm
$Na^{10}B_5O_8$	2.06*	2.98 µm	5.88 µm	2.66 µm	4.82 µm
^{10}BN	2.10	2.61 µm	5.21 µm	2.34 µm	4.24 µm
		^{3}H (2.73 MeV)	α (2.05 MeV)		
^{6}LiF	2.64	62.7 µm	6.04 µm		
		IC_{e^-} (29 keV)	IC_{e^-} (71 keV)	**Experimentally measured by Steven Cool*	
$^{157}Gd_2O_2S$:Tb	7.32	1.31 µm	5.46 µm		

The density of $Na^{10}B_5O_8$ has been measured experimentally by Steven Cool, as indicated with an asterisk at the value itself (2.06 *) and an asterisk at the lower right of teh table, mentioning the explanation

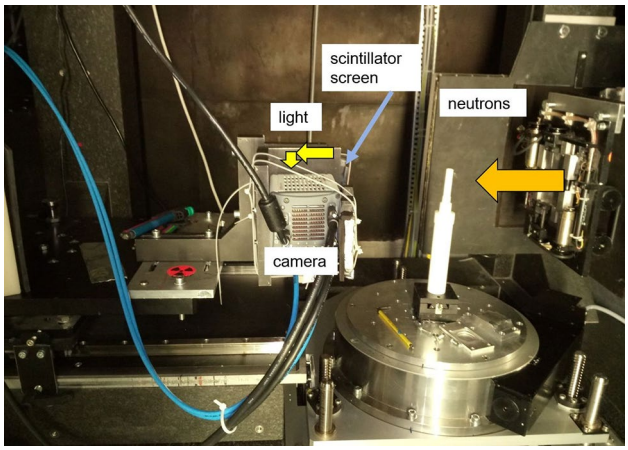

Fig. 1 Setup at NeXT Grenoble

All images clearly show that the powder was not as homogeneously milled as expected, and many large grains are interspersed on the surface. However, in homogenous areas, a resolution on the order of 10–11 µm can be observed for the 20 µm thick borated screens, which matches the resolution of the reference screen made of 10 µm Gadox in Fig. 4. Screen resolution was measured with an inclined Gd edge as shown in Fig. 5 to determine the edge spread function and derive the modulation transfer function (MTF).

Detection efficiency, light output and resolution measurements

To measure detection efficiency, the borated screens were mounted as absorbing samples on the outside of the Gadox reference screen, as shown in Fig. 6. Both Gd and B show a 1/v absorption behavior in the cold and thermal neutron energy range, so this method is valid as discussed in [19]. Table 2 shows the experiment parameters and Table 3 shows the measured results in light output, detection efficiency, and spatial resolution.

The reference screen was a 10 µm thick ^{157}Gd-enriched Gadox screen made by RC Tritec [20]. Two types of screens were measured, containing ZnS:Cu as phosphor and ^{10}B-enriched boron oxide, $^{10}B_2O_3$, or sodium pentaborate, $Na^{10}B_5O_8$, as converter material, each type with 2:1 and 1:1 mixing ratio (converter atoms to scintillator molecules). Screen thickness was measured several times by two persons using an eddy current probe, and the measurements were averaged together.

The most captivating result is that all screens render a spatial resolution very close to the 10 µm Gadox reference screen (Fig. 7, 32.2–40.4 lp/mm, or 24.8–31.0 µm for a line pair), even though their thickness varies from four to seven times the thickness of the reference screen. This is a clear indication that the average range of the reaction products is very small (a few µm) and is at first sight not influenced by the available screen thickness; also, the optical dispersion of the scintillation light does not seem to significantly influence the spatial resolution. This is a possible indication that screen thickness may be increased for increased detection efficiency without losing spatial resolution—new screens up to 200 µm thickness must be tested in the future. Producing thinner borated screens (~ 10 µm thick) might theoretically produce even better effective spatial resolution, but would provide much lower detection efficiency.

The second noticeable result is that most screens provide a higher light output than the reference screen, some more than two times as much. This is especially remarkable since the calculated detection efficiency for these screens is only on the order of 6–19%, with 6.4–13.4% calculated for a 50 µm thick reference screen, while the detection efficiency for the 10 µm Gadox screen should be more than 90%. The relative grey level per detected neutron in the detector is only 0.5 to 1.0, which means that the detected neutrons are undersampled in the detector signal. This also implies that neutrons detected by the Gadox screen are undersampled about 20 times more. For the noise behavior of a detection system, the neutron statistics are the most important parameter as long as there are several photons detected per neutron. If the number of detected photons per detected neutron is about the same, the photon statistics influence the signal just as much as

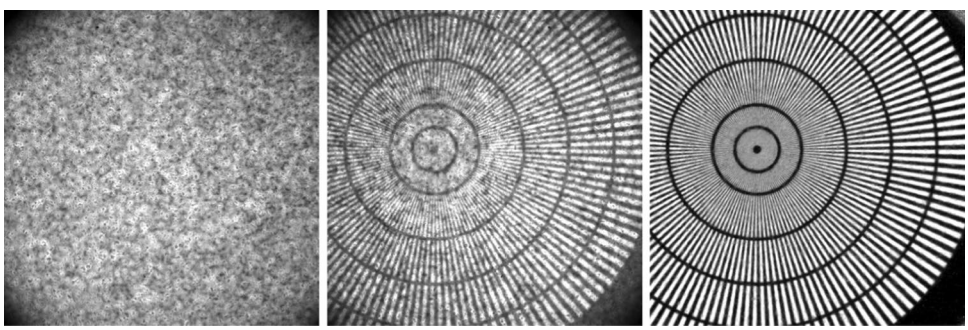

Fig. 2 Images taken with Screen C72-08 (Table 2) showing an open beam, Siemens star, and normalized Siemens star

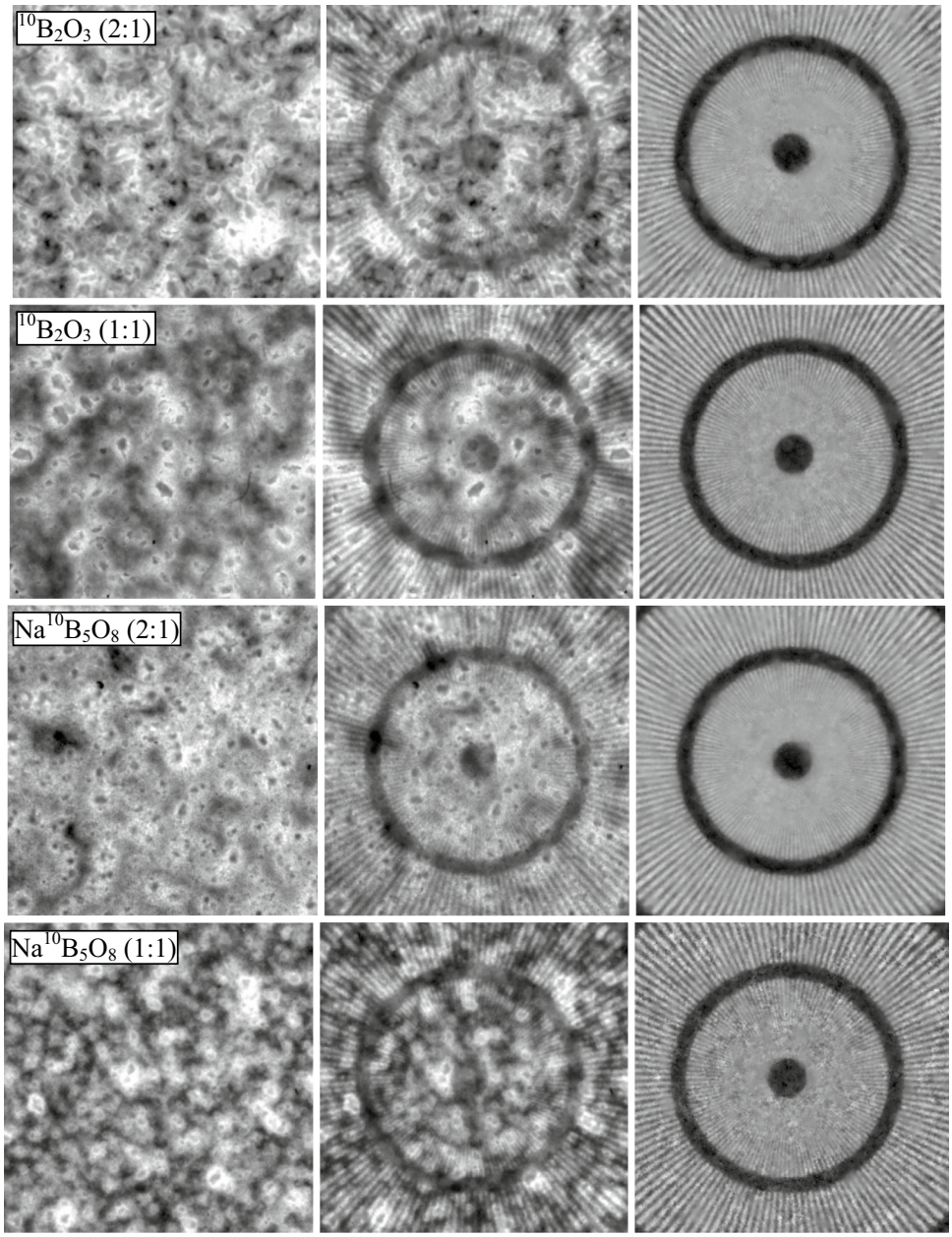

Fig. 3 Borated screen images: open beam, Siemens star, and normalized Siemens star with 3.6 µm pixel size for $^{10}B_2O_3$ (2:1), $^{10}B_2O_3$ (1:1), $Na^{10}B_5O_8$ (2:1) and $Na^{10}B_5O_8$ (1:1)

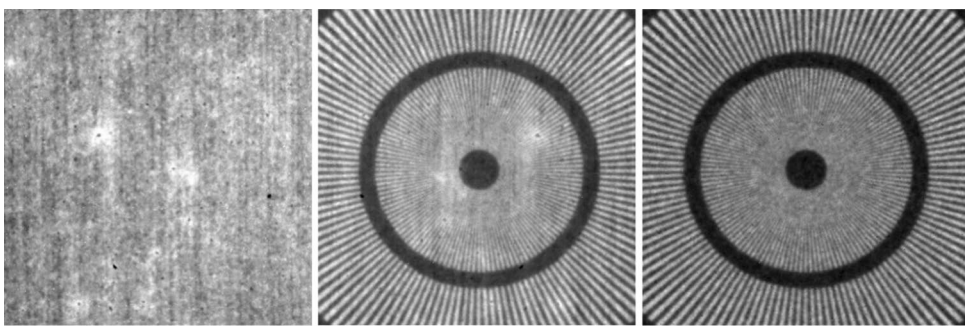

Fig. 4 10 µm Gd reference screen images: Open beam, Siemens star, and normalized Siemens star with 3.6 µm pixel size

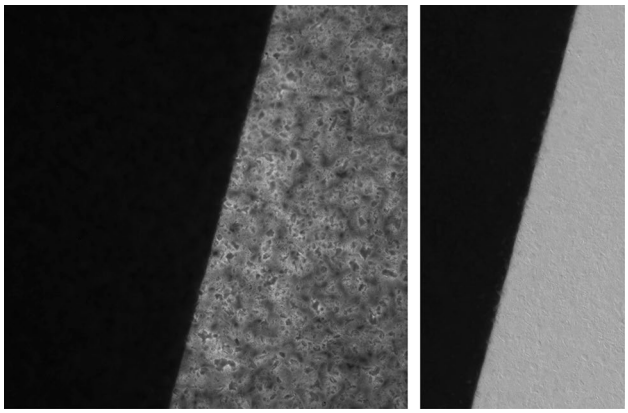

Fig. 5 Neutron radiograph of a gadolinium edge on Screen C72-08 to determine resolution prior to (left) and after (right) open beam correction and cropping

the neutron statistics. [21] Neutron detectors using optical cameras must thus strive to detect several photons of the several thousand photons emitted into 4π space by a detection event.

SEM measurements of the screens

Since the neutron measurements apparently showed large grains of converter material, the screens were examined with a scanning electron microscope (SEM) after the neutron measurements to prove the existence of large particles. The measurements show that the structure of the powders is comprised of completely different shapes—all of which demand finer milling, and particle size separation. Figure 8 shows SEM images of $^{10}B_2O_3 + ZnS:Cu$ at 40×, 100×, 500× and 1000× magnification. There are several relatively large agglomerates as well as needle crystals. Sieving out the larger grains and crushing the needle crystals to increase screen homogeneity is planned for the next batch of screens.

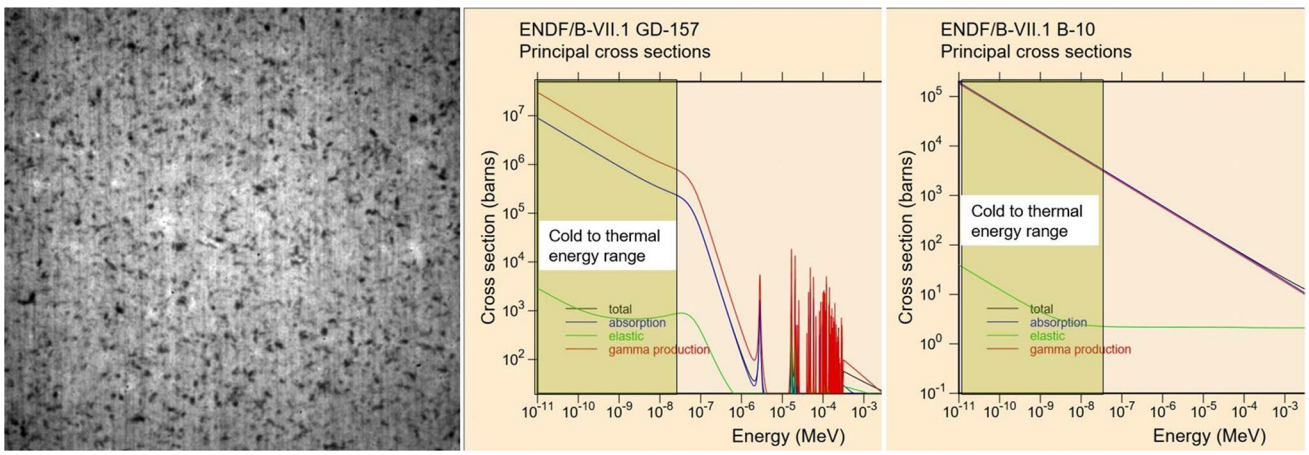

Fig. 6 Example of a radiograph of ^{10}B-based screen C72-01 on the Gd reference screen, and the cross sections for ^{157}Gd and ^{10}B from the ENDF B-VII data base

Table 2 Screen parameters

Screen ID#	Description	Areal thickness (mg/cm^2)	Measured thickness(μm) [1]	STDEV	Coating density(g/cm^3)
	10 μm Gadox from RC Tritec	–	10		
C72-07	$^{10}B_2O_3$ (2:1) ZnS:Cu	4.33	68.85	8.56	0.629
C72-08	$^{10}B_2O_3$ (2:1) ZnS:Cu	6.06	73.40	3.92	0.826
C72-15	$^{10}B_2O_3$ (1:1) ZnS:Cu	6.06	46.70	5.66	1.298
C72-16	$^{10}B_2O_3$ (1:1) ZnS:Cu	5.19	40.83	7.90	1.271
C72-23	$Na^{10}B_5O_8$ (2:1) ZnS:Cu	6.06	72.60	7.08	0.835
C72-24	$Na^{10}B_5O_8$ (2:1) ZnS:Cu	6.06	71.93	5.44	0.843
C72-31	$Na^{10}B_5O_8$ (1:1) ZnS:Cu	3.46	46.60	9.66	0.742
C72-32	$Na^{10}B_5O_8$ (1:1) ZnS:Cu	3.46	42.35	5.43	0.817

Table 3 Measured results for light output, detection efficiency, and spatial resolution

Light output		Detection efficiency				Resolution			
Avg. Brightness of Flat-Field	STDEV	Avg. detection efficiency	STDEV	Det. eff. of a 50 µm thick screen	Graylevels per neutron	Relative Graylevels per neutron	Pixel size(µm)	Pixels per mm	Nyquist frequency(lp/mm)	lp/mm at 10% MTF
12,520	1360						3.58	279.7	139.9	38.6
19,646	5535	12.6%	0.96%	9.2%		0.57	3.58	279.7	139.9	33.5
27,225	5770	15.6%	1.26%	10.6%		0.64	3.58	279.7	139.9	32.2
16,297	4467	6.8%	0.38%	7.3%		0.88	3.58	279.7	139.9	40.3
17,197	4526	6.3%	0.34%	7.7%		1.00	3.58	279.7	139.9	37.9
27,787	5164	19.4%	1.66%	13.4%		0.52	3.58	279.7	139.9	37.4
25,632	5130	19.3%	1.63%	13.4%		0.49	3.58	279.7	139.9	38.3
9282	3639	6.0%	0.35%	6.4%		0.57	3.58	279.7	139.9	39.8
9333	3603	6.1%	0.36%	7.2%		0.56	3.58	279.7	139.9	40.4

Figure 9 shows SEM images of $Na^{10}B_5O_8 + ZnS:Cu$ at 40×, 100×, 500× and 500× magnification. They show agglomerates of small and large grains, with large grains up to 120 µm size, and agglomerates up to 240 µm size composed of much smaller grains from 10 to 50 µm size. The task for better processing will be to break up the agglomerates, then sieve out the remaining large single grains.

Neutron computed tomography

One neutron computed tomography scan was performed using screen C72-23, showing rear section and part of the torso of an insect, sitting on a small snail shell. Eight hundred projections, with an acquisition time of 8 s each, were recorded over 180° with a 2048 × 2048 pixel array. The left of Fig. 10 shows an arbitrary slice of the insect body. Since the contrast is very low, the reconstruction is noisy, and measuring details within the slice is difficult. The right side shows a 3D reconstruction of the insect and snail shell. The snail shell is about 6.6 mm wide. Even with the current graininess, the screens are already fit for use in high resolution measurements.

Conclusion and outlook

Borated screens matched the resolution of a reference Gadox screen despite being double the thickness and having 50% the detection efficiency of Gadox, but two times the light output. The remaining problems in development are of a mechanical nature—powders must be milled more finely, and the particle sizes in the coatings made more homogeneously. Borated neutron imaging screens will fill a gap between Gadox and ZnS screens for very high resolution neutron imaging.

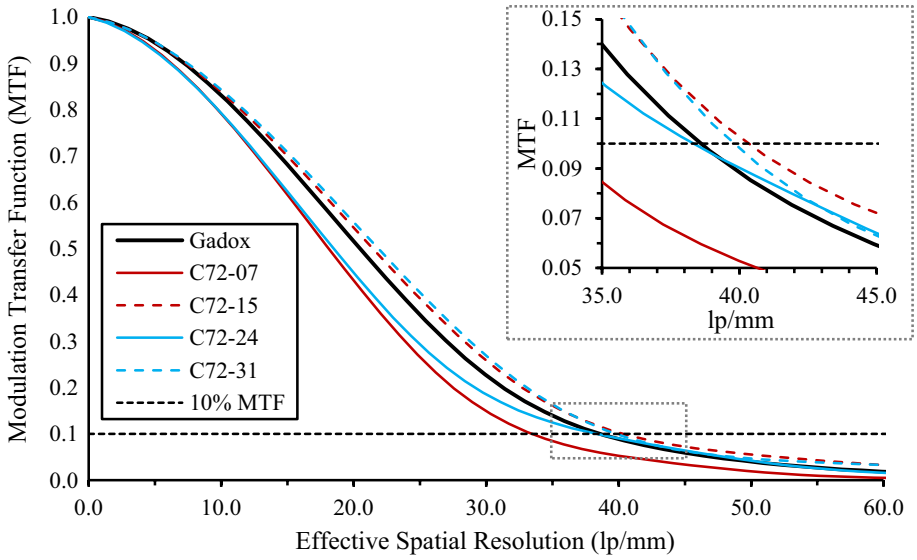

Fig. 7 Measured spatial resolution for all screens is very similar

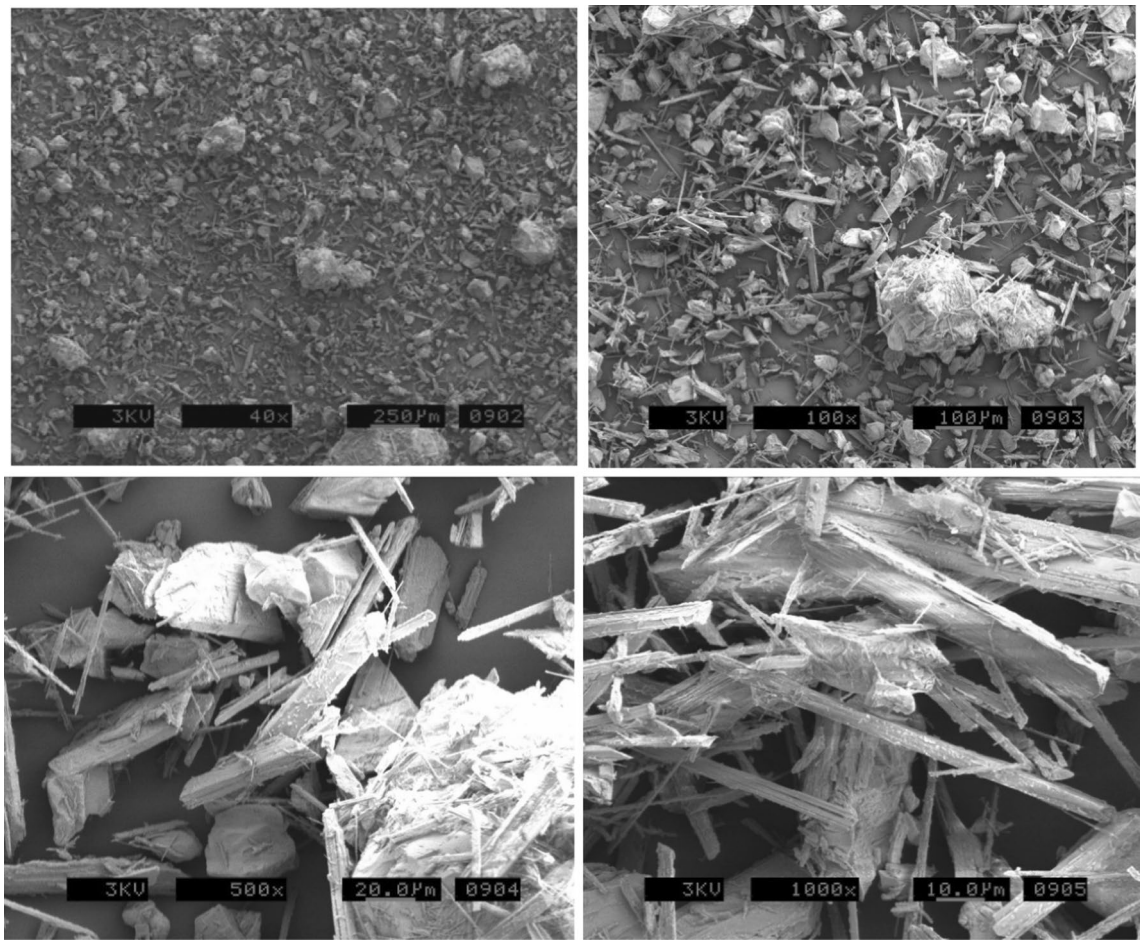

Fig. 8 SEM images of $^{10}B_2O_3$ + ZnS:Cu at 40×, 100×, 500× and 1000× magnification, showing agglomerates as well as needle crystals

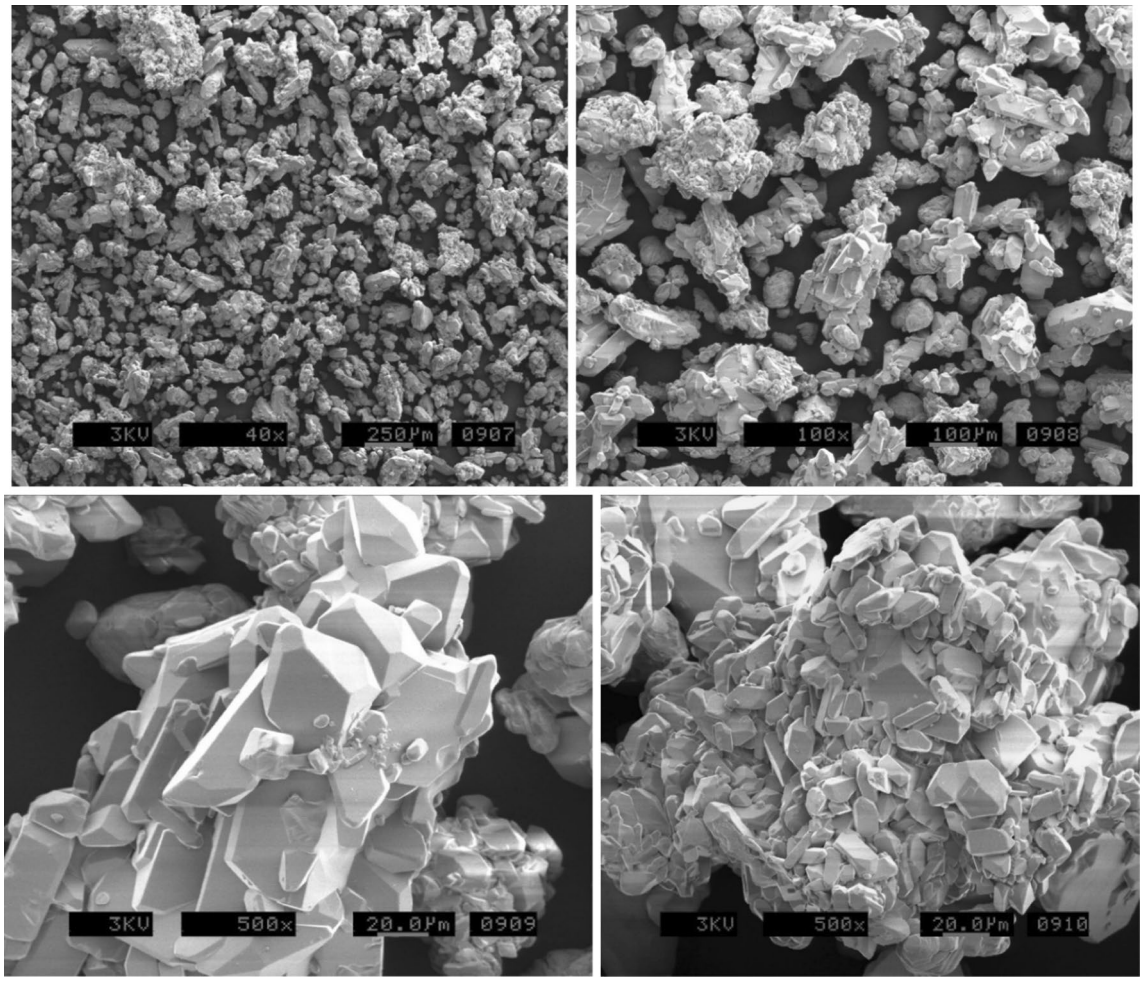

Fig. 9 SEM images of $Na^{10}B_5O_8 + ZnS:Cu$ at 40×, 100×, 500× and 500× magnification, showing agglomerates as well as large grains

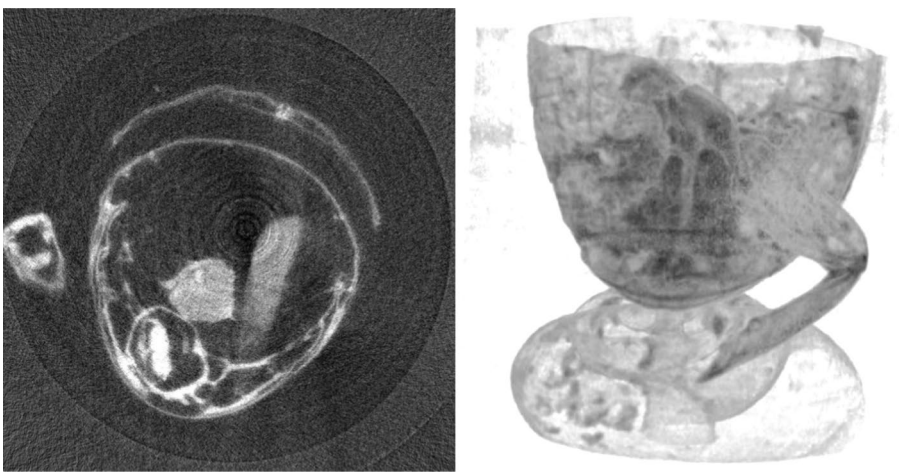

Fig. 10 Neutron computed tomography of the rear section of an insect on a snail shell, single slice of the insect body and 3D reconstruction of both. The snail shell is about 6.6 mm wide

Acknowledgements Work funded through the INL Laboratory Directed Research & Development (LDRD) Program under DOE Idaho Operations Office Contract DE-AC07-05ID14517, LDRD Project ID# 20A44-200FP.

Funding Open Access funding enabled and organized by Projekt DEAL.

References

1. Stedman R (1960) Scintillator for thermal neutrons using Li6F and ZnS (Ag). Rev Sci Instrum 31(10):1156–1156
2. Knoll GF (2010) Radiation detection and measurement. Wiley
3. Crha J, Vila-Comamala J, Lehmann E, David C, Trtik P (2019) Light yield enhancement of 157-gadolinium oxysulfide scintillator screens for the high-resolution neutron imaging. MethodsX 6:107–114
4. Chuirazzi W, Craft A, Schillinger B, Cool S, Tengattini A (2020) Boron-based neutron scintillator screens for neutron imaging. J Imaging 6(11):124
5. McGonnagle WJ (1960) Symposium on Physics and Nondestructive Testing
6. Kojima T, Katagiri M, Tsutsui N, Imai K, Matsubayashi M, Sakasai K (2004) Neutron scintillators with high detection efficiency. Nucl Instrum Methods Phys Res, Sect A 529(1–3):325–328
7. Katagiri M, Sakasai K, Matsubayashi M, Kojima T (2004) Neutron/γ-ray discrimination characteristics of novel neutron scintillators. Nucl Instrum Methods Phys Res, Sect A 529(1–3):317–320
8. Ishii M, Kuwano Y, Asai T, Asaba S, Kawamura M, Senguttuvan N, Shimizu HM (2005) Boron based oxide scintillation glass for neutron detection. Nucl Instrum Methods Phys Res, Sect A 537(1–2):282–285
9. Nguyen LQ, Gabella G, Goldblum BL, Laplace TA, Carlson JS, Brubaker E, Feng PL (2021) Boron-loaded organic glass scintillators. Nucl Instrum Methods Phys Res, Sect A 988:164898
10. Normand S, Mouanda B, Haan S, Louvel M (2002) Discrimination methods between neutron and gamma rays for boron loaded plastic scintillators. Nucl Instrum Methods Phys Res, Sect A 484(1–3):342–350
11. Britvich GI, Vasil'Chenko VG, Gilitsky YV, Chubenko AP, Kushnirenko AE, Mamidzhanyan EA, Shepetov AL (2005) A neutron detector on the basis of a boron-containing plastic scintillator. Nucl Instrum Methods Phys Res, Sect A 550(1–2):343–358
12. Mahl A, Yemam HA, Stuntz J, Remedes T, Sellinger A, Greife U (2016) Bis (pinacolato) diboron as an additive for the detection of thermal neutrons in plastic scintillators. Nucl Instrum Methods Phys Res, Sect A 816:96–100
13. Mahl A, Yemam HA, Fernando R, Koubek JT, Sellinger A, Greife U (2018) 10B enriched plastic scintillators for application in thermal neutron detection. Nucl Instrum Methods Phys Res, Sect A 880:1–5
14. Verhaeghe JL, Thielens G, Creten WL (1962) Preparation and properties of a boron containing scintillator for the detection of slow neutrons. Appl Sci Res Sect B 10(3):247–256
15. Brenizer JS, Berger H, Stebbings CT, Gillies GT (1997) Performance characteristics of scintillators for use in an electronic neutron imaging system for neutron radiography. Rev Sci Instrum 68(9):3371–3379
16. McMillan JE, Cole AJ, Kirby A, Marsden E (2015) Thermal neutron scintillators using unenriched boron nitride and zinc sulfide. J Phys Conf Ser 620:012011
17. Schulz M, Schillinger B (2015) ANTARES: cold neutron radiography and tomography facility. J Large-Scale Res Facil JLSRF 1:17
18. Tengattini A, Lenoir N, Andò E, Giroud B, Atkins D, Beaucour J, Viggiani G (2020) NeXT-Grenoble, the neutron and X-ray tomograph in Grenoble. Nucl Instrum Methods Phys Res, Sect A 968:163939
19. Chuirazzi WC, Craft AE (2020) Measuring thickness-dependent relative light yield and detection efficiency of scintillator screens. J Imaging 6(7):56
20. https://www.rctritec.com/en/scintillators/products.html
21. Schillinger B, Saha S (2017) The signal chain—how the removal of an image intensifier at the AERE reactor in Bangladesh improves neutron imaging. Phys Proc 88:243–249